Bull. Chem. Soc. Ethiop. **2025**, 39(8), 1509-1523.
DOI: https://dx.doi.org/10.4314/bcse.v39i8.5

ISSN 1011-3924
Printed in Ethiopia
Online ISSN 1726-801X

PREPARATION, KINETICS, AND THERMODYNAMIC INVESTIGATION OF JANUS GREEN DYE REMOVAL FROM AQUEOUS SOLUTIONS USING MnO_2 NANOPARTICLES AS AN ADSORBENT

Nagham Hameed Abood[1] and Sundus Hadi Merza[2*]

[1]Department of Applied Science, Applied Chemistry, University of Technology, Baghdad, Iraq
[1,2]Department of Chemistry, College of Education for Pure Science, Ibn-Al-Haitham, University of Baghdad, Iraq

(Received January 24, 2025; Revised March 28, 2025; Accepted April 28, 2025)

ABSTRACT. In this study, manganese dioxide (MnO_2) nanoparticles (NPs) were synthesized via the hydrothermal method and utilized for the adsorption of Janus green dye (JG) from aqueous solutions. The effects of MnO_2 NPs on kinetics and diffusion were also analyzed. The synthesized NPs were characterized by scanning electron microscopy (SEM), X-ray diffraction (XRD), energy-dispersive X-ray analysis (EDX), and Fourier-transform infrared spectroscopy (FT-IR), with XRD confirming the nanoparticle size of 6.23 nm. The adsorption kinetics were investigated using three models: pseudo-first-order (PFO), pseudo-second-order (PSO), and the intraparticle diffusion model. The PSO model provided the best fit ($R^2 = 0.999$), indicating that the adsorption process is chemical in nature. Kinetic analysis revealed that the MnO_2 surface exhibited faster adsorption kinetics during the film diffusion step (rate constant 0.2776) compared to intraparticle diffusion (0.0042) at 298.15 K. Thermodynamic parameters, including enthalpy change (ΔH^*), entropy change (ΔS^*), and Gibbs free energy change (ΔG^*) of activation, were calculated from the Eyring equation to be 37.48 kJ/mol and -144.69 J/mol, respectively. The positive ΔG^* value (80.62 kJ/mol) suggests that the adsorption process is energy-intensive, requiring higher energy to form chemical bonds between JG and MnO_2 nanoparticles.

KEY WORDS: Hydrothermal method, Janus green dye, Manganese dioxide nanoparticles, Kinetic behavior, Intraparticle diffusion model

INTRODUCTION

Many countries in the world, especially developing ones, have turned their attention to the problem of water pollution with pollutants which may be organic or inorganic compounds due to their negative effects on the environment and human health [1]. Among the most dangerous of these pollutants are dyes, due to their global production in large quantities that may reach millions of tons from many various industries such as textile, food, cosmetics, and leather industries [2]. Thus, it is necessary to remove these dyes from their effluents before they flow into water sources that are daily used by humans in drinking, cooking, and washing [3, 4]. Dyes are complex chemical compounds with high thermal and chemical stability, which makes many of them non-biodegradable naturally through light, heat, or natural oxidizing agents [5].

The set free of dye effluents into water can disrupt aquatic life, causing serious harm to organisms due to the reduction in photosynthesis. These effluents often contain mutagenic, carcinogenic, or toxic chemicals that threaten aquatic species. Additionally, the presence of dyes or their by-products in water can lead to human health issues such as nausea, skin ulceration, and damage to mucous membranes and central nervous systems. Therefore, many physical, chemical, and biological techniques have been used to remove these pollutants from their aqueous solutions, such as ozonation [6], separation of membranes [7], ultrafiltration membrane [8], electrodialysis [9], electrocoagulation [10], coagulation-flocculation [11]and treatment by adsorption [12]. However, many of these techniques are costly, particularly for large-scale wastewater treatment.

*Corresponding authors. E-mail: sundus.h.m@ihcoedu.uobaghdad.edu.iq

Consequently, adsorption technology is one of the most widely used techniques for wastewater treatment due to its high efficiency in removing pollutants, economy, and ease of application. Additionally, it can be used for a large number of compounds [13]. Therefore, many materials were tested as adsorbents, like carbonaceous materials, biosorbents, activated carbon nanotubes, and nanomaterials to remove dye particles from their aqueous solutions.

Nanomaterials have multiple unique chemical and physical properties, like strong chemical reactivity, catalytic ability, conductivity, and magnetism. Thus, nanomaterials are employed as nano-adsorbents in various forms, including particles, clays, fibers, carbon-based materials, and metals, for water purification from contaminant [14]. Researchers in the nanotechnology aspect are increasingly focusing on manganese dioxide (MnO_2) due to its high activity, affordability, non-toxicity, impressive specific capacitance, diverse structures, and morphologies, as well as its wide range of applications in chemical sensing, lithium batteries, supercapacitors, and catalysis. Many studies have also focused on improving the catalytic activity of MnO_2 by combining it with other materials [15-17]. Several studies have demonstrated that MnO_2 is an effective adsorbent with a high capacity for removing dyes from wastewater, and it is also environmentally benign [18, 19]. Therefore, this study aims to explore the potential of MnO_2 nanoparticles as an adsorbent for Janus Green dye (JG), a cationic dye known for its dark green color and stability across a wide pH range. JG is commonly used in histology to stain chromosomes, nucleic acids, mitochondria, and fungi in living tissues [20]. Although MnO_2 has been studied for the adsorption of various pollutants, its application specifically for JG dye remains underexplored, making this research a unique contribution to the field of water treatment.

EXPERIMENTAL

Chemical and materials

Manganese sulfate ($MnSO_4 \cdot 4H_2O$, 95%) and potassium permanganate ($KMnO_4$, 99%) were obtained from BDH (England) and Merck (Germany), respectively, as raw materials for preparing MnO_2 nanoparticles. Janus Green dye (JG, $C_{30}H_{31}ClN$, molecular weight = 511.06 g/mol, λ_{max} = 611 nm, pH = 7) was sourced from Hopkin and Williams Ltd., England as the adsorbate. Nitric acid (69–72%) was supplied by Central Drug House (CDH), India, and used as the catalyst reagent. Distilled water was used to prepare all working solutions.

Instruments

The adsorption process data were measured using a Hettich centrifuge (EBA-20), a Sartorius laboratory balance (L420 B), a Shimadzu UV/Vis spectrophotometer (UV-1800), and a Labtech shaker water bath with temperature control. The structural characteristics of MnO_2 were analyzed using XRD-6000 (Shimadzu, Japan) along with EDX spectroscopy (MIRA3, TESCAN, Czech Republic). The materials' size and shape were examined using scanning electron microscopy (SEM, Hitachi S-4800FEG). FT-IR spectrophotometer (Shimadzu 8400S, Japan), with a range of 400 to 4000 cm^{-1}, was used to characterize MnO_2 structure.

Synthesis of MnO_2

About 37.02 g of $MnSO_4 \cdot 4H_2O$ were dissolved in 50 mL of distilled water to form a saturated salt solution. Similarly, 2.37 g of $KMnO_4$ was dissolved in 50 mL of distilled water to prepare a 0.3 M $KMnO_4$ solution, which was then gradually added to the aqueous manganese sulfate solution. Two drops of HNO_3 were added to the reaction mixture as a catalyst. The mixture was heated to 80 °C using a hot plate and stirred with a magnetic stirrer for 2 h. The mixture was then transferred to a beaker and placed in an ultrasonic device for 1 h at room temperature. The resulting black

solution was filtered, washed several times with distilled water, and then dried at 80 °C for 6 h. The resulting material was ground before characterization and used in the adsorption process. The formation of MnO_2 nanoparticles is explained according to Eq. 1 and Eq. 2 [21]:

$$2H_2O \rightarrow 4H^+_{aq} + O_{2(g)} + 4e^- \quad (1)$$

$$MnO^-_{4(aq)} + 4H^+ + 3e^- \rightarrow MnO_{2(S)} + 2H_2O \quad (2)$$

FT-IR analysis

In this study, the FT-IR spectrum was recorded in the range of 400-4000 cm^{-1} for the MnO_2 surface before and after the adsorption of JG dye. The FT-IR spectrum allowed us to identify the distinctive peaks corresponding to the active groups present on the studied surface.

XRD analysis

The structural and crystallographic properties of MnO_2 were estimated using XRD diffraction. The crystalline size (D) of the MnO_2 nanoparticles was determined using the Debye-Scherrer equation (Eq. 3), where 0.94 and λ are the shape factor and wavelength of X-rays (0.1543 nm), respectively.

$$D = \frac{0.94\lambda}{\beta_D cos\theta} \quad (3)$$

FE-SEM

Morphological analysis of the MnO_2 sample before and after JG dye adsorption was conducted using FE-SEM at a 60 KX magnification and a size scale of 200 nm.

Energy dispersive X-ray technique (EDX)

In this study, the EDX spectrum of the MnO_2 surface before and after the adsorption process was recorded.

RESULTS AND DISCUSSION

MnO_2 NPs characterization

FT-IR analysis

The FT-IR spectrum for the MnO_2 surface before and after adsorption of JG dye are shown in Figures (1a, b), respectively. The FT-IR spectrum of MnO_2 nanoparticles before the adsorption of JG dye (Figure 1a) shows characteristic bands corresponding to Mn-O bond stretching at 455 and 503 cm^{-1}. Additionally, the peak at 703 cm^{-1} corresponds to the stretching mode of MnO_6 octahedra along the double chain [21, 22]. The –OH stretching vibration and the scissoring mode of absorbed water molecules appear at frequencies 3426 cm^{-1} and 1615 cm^{-1}, respectively [23]. After the adsorption of JG dye (Figure 1b), new peaks appear around 1381 cm^{-1}, which correspond to the stretching vibrations of the C-N bond in aromatic tertiary amines [24]. The peak at 1472 cm^{-1} corresponds to the stretching vibrations of the C=C bond. The stretching vibration of azo groups shows absorption close to the double bond stretching region. The presence of these new peaks, along with shifts in existing ones, indicates the successful interaction between MnO_2 nanoparticles and JG dye.

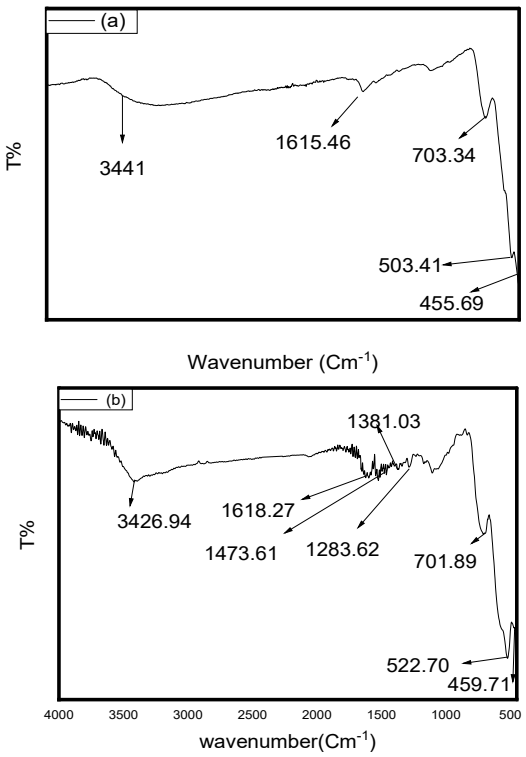

Figure 1. FT-IR spectrum of MnO_2 adsorbent (a) before and (b) after adsorption JG.

XRD analysis

The XRD pattern of MnO_2, presented in Figure 2, reveals diffraction peaks at 12.88°, 18.57°, 28.60°, 37.5°, 42.13°, 49.88°, 56.22°, 60.08°, 69.14°, and 72.7°. These peaks correspond closely to the diffraction patterns of the crystal planes of α-MnO_2, as indicated by the standard data from Joint Committee on Powder Diffraction Standards (JCPDS) card No. 44-0141 [25,26]. By using the strongest diffraction peak (211), with a diffraction angle (θ) of 18.7766° and a full width at half maximum (β) of 0.0235 rad, the size of the MnO_2 nanoparticles was calculated to be 6.23 nm.

FE-SEM

The morphological analysis of the MnO_2 sample before and after JG dye adsorption conducted using FE-SEM at 60 KX was shown in Figures (3a, b). The MnO_2 nanoparticles before JG dye adsorption appear as heterogeneous rod-shaped structures with varying sizes, forming agglomerates in the shape of clusters, with an average size of less than 42 nm (Figure 3a). In comparison, the FE-SEM image of MnO_2 nanoparticles after adsorption (Figure 3b) shows a noticeable reduction in size (less than 32 nm) and a more uniform coverage of the adsorbent surface. This change can be attributed to the de-aggregation of the nanoparticles caused by interaction with the dye molecules. These observations are consistent with the kinetic investigation and activation energy values. Additionally, the size measured by FE-SEM is larger than that calculated using the Debye-Scherrer equation, which may be due to the formation of agglomerates.

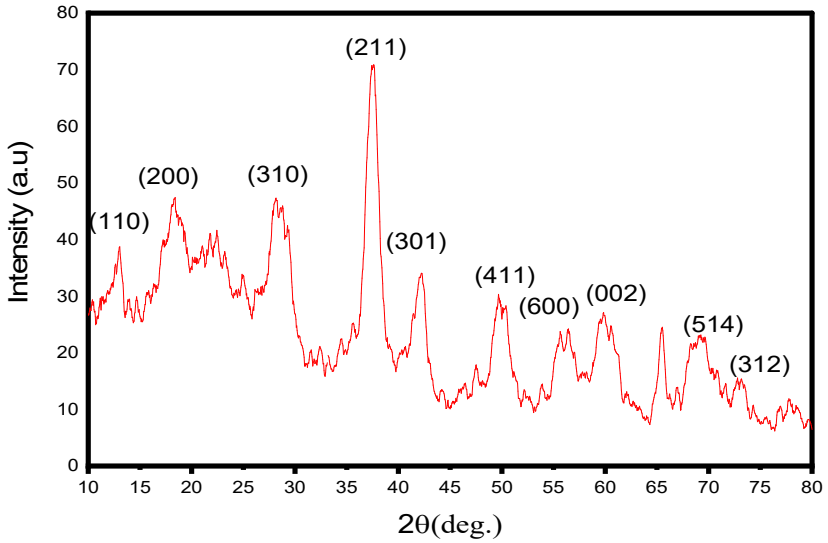

Figure 2. XRD pattern of MnO_2 nanoparticles.

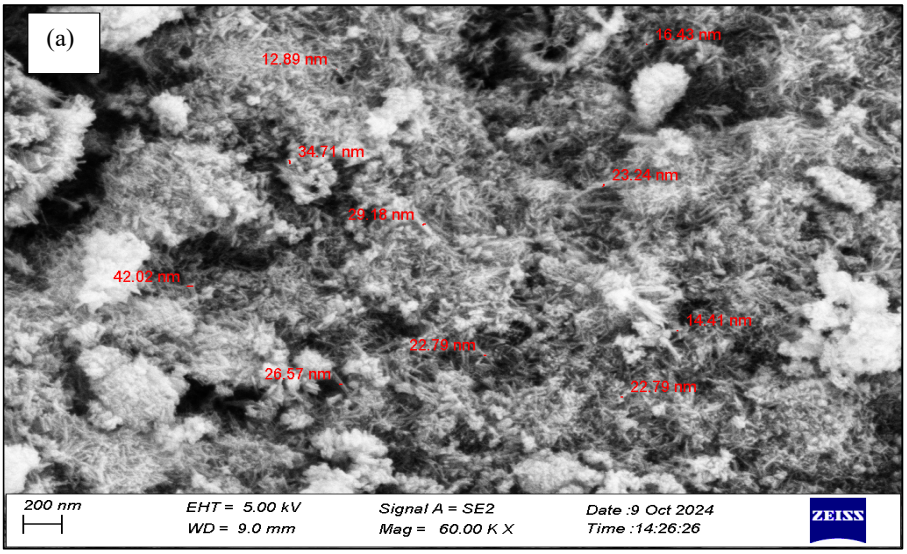

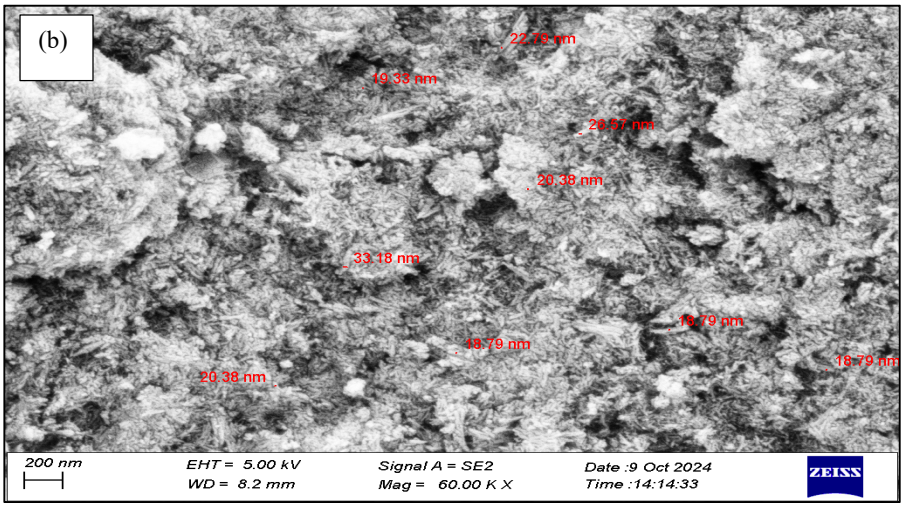

Figure 3. SEM of MnO_2 adsorbent (a) before (b) after adsorption of JG dye at scale 200 nm and 60 kx magnification.

Energy dispersive X-ray technique (EDX)

The EDX spectrum of the MnO_2 surface before and after the adsorption process was recorded in Figure 4, and the surface of MnO_2 before dye adsorption is primarily composed of manganese and oxygen, with trace amounts of potassium and sulfur, which are residuals from the reacting materials (Figure 4a). A small amount of carbon, likely from impurities, was also detected. After adsorption of the JG dye (Figure 4b), new peaks corresponding to the elements of the dye namely nitrogen, carbon, and chlorine appear, in addition to the peaks associated with the MnO_2 surface elements. This confirms the successful adsorption of JG dye from its aqueous solution onto the MnO_2 surface.

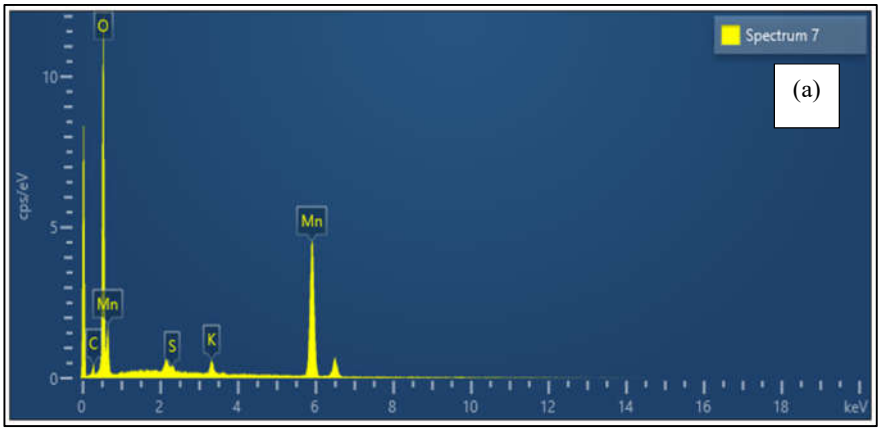

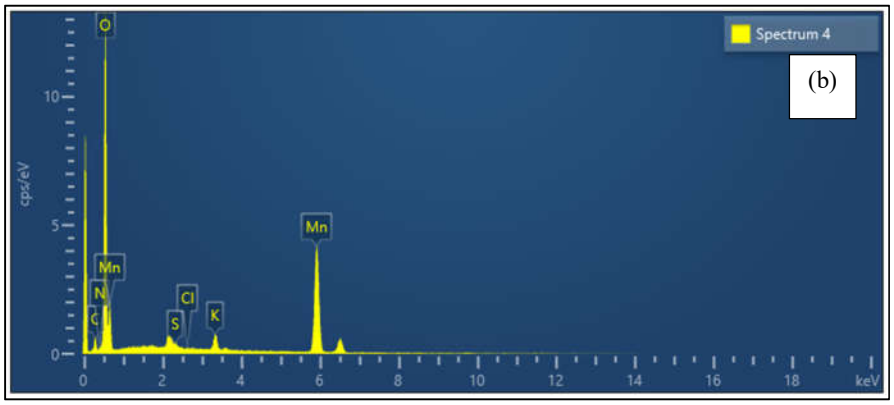

Figure 4. EDX of MnO_2 (a) before and (b) after adsorption of JG dye.

Calibration curve for the JG dye

The calibration curve for the JG dye was established by preparing a series of solutions with varying concentrations (3, 6, 9, 12, 15, 18, 21, 24, 27, 30, 33, 36, and 42 mg/L). The absorbance of these dye solutions was measured using a UV-vis spectrophotometer at 611 nm. The absorbance values were then plotted against the corresponding concentration values using Beer-Lambert's law, as shown in Figure 5.

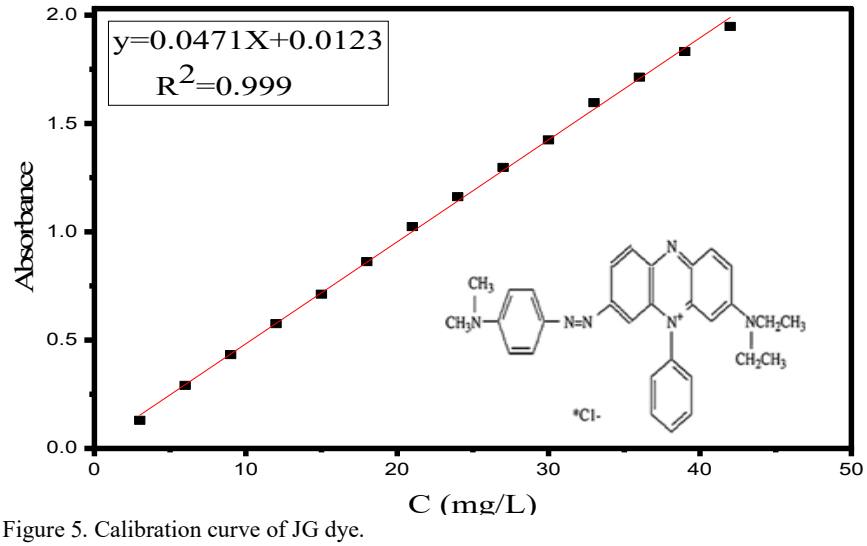

Figure 5. Calibration curve of JG dye.

Adsorption experiment

Different weights of MnO_2 (0.005, 0.015, 0.025, 0.035, 0.045, 0.055, 0.065, 0.075, 0.1, and 0.15 g) were mixed with 10 mL of JG dye solution (42 mg/L) in ten round flasks. The flasks were shaken in a water bath shaker at 150 rpm for 1h at 25 °C. Afterward, the dye solution was

separated from the adsorbent surface by centrifugation. The absorbance of the dye solution was measured using a UV-vis spectrophotometer. The removal efficiency (R%) of JG dye was then calculated using the following equation [27, 28]:

$$R\% = \frac{C_o - C_e}{C_o} \times 100 \quad (4)$$

The initial and equilibrium concentrations of JG dye are represented by C_o and C_e (mg/L), respectively. The experiments were conducted over a temperature range (15 °C, 25 °C, 35 °C, and 45 °C) and for different times (5–180 min), using 0.15 g of MnO_2 and an initial JG dye concentration of 42 mg/L. The amount of JG dye adsorbed on the MnO_2 at time t, denoted as q_t (mg/g), was determined using the following equation [29, 30]:

$$q_t = \frac{V\,(C_o - C_t)}{m} \quad (5)$$

where V (L) is the volume of adsorbent material, m (g) is the weight of MnO_2, and the concentrations of JG dye before and after adsorption are expressed as C_o and C_t (mg/L), respectively.

Effect of adsorbent dose

The amount of adsorbent used is a key factor in determining the efficiency of the adsorption process. This relationship was demonstrated by plotting the removal percentage of JG dye (R%) against the weight of MnO_2 as the adsorbent, as shown in Figure 6. The removal percentage (R%) of JG dye increases as the adsorbent weight increases. It also highlights that MnO_2 achieves the highest removal rate of JG dye, reaching 87.55% with a relatively low dosage of 0.15 g. This low dosage is more cost-effective compared to the study conducted by Donk [31]. The high efficiency at this low dosage can be attributed to the large surface area and the numerous active sites on the MnO_2 particles.

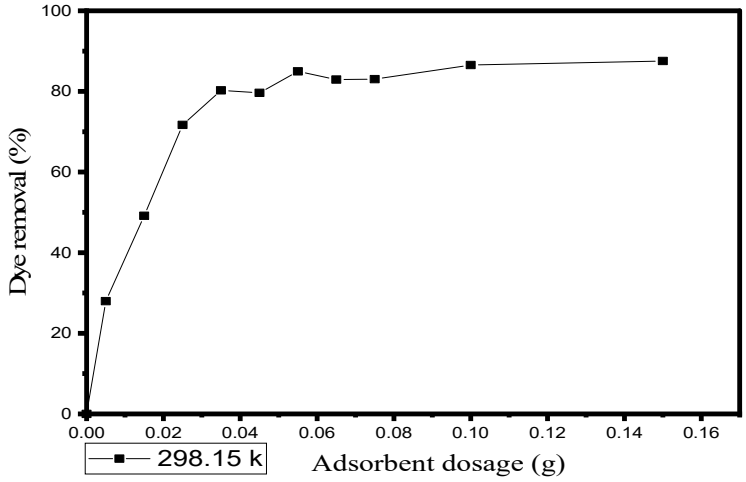

Figure 6. Removal percentage of JG dye vs. the weight of MnO_2.

Effect of contact time and temperature on JG dye adsorption

The influence of contact time and temperature on the adsorption of JG dye (42 mg/L) onto MnO_2 was investigated to optimize the removal efficiency (Figure 7). Contact time was varied from 5 to 180 min, and the removal percentage (R%) of JG dye was plotted against time. The results indicated that the removal efficiency increased with time, reaching a maximum of 60 min [31], suggesting the saturation of active sites on the adsorbent. The effect of temperature was also studied by examining dye removal at four different temperatures (15, 25, 35, and 45 °C). The results showed a significant increase in removal efficiency from 76.20% at 15 °C to 86.80% at 45 °C, indicating a temperature-dependent enhancement in the adsorption process. This increase in efficiency is attributed to the elevated diffusion rate of the adsorbate molecules into the MnO_2 particles, supporting the hypothesis that the adsorption process is endothermic [18].

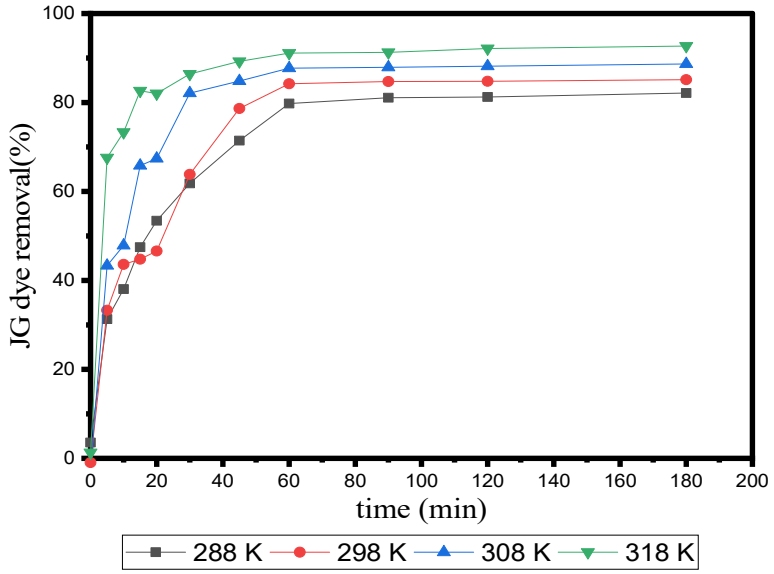

Figure 7. The effect of temperatures on the adsorption rate of JG dye by MnO_2.

Kinetic study

To evaluate the kinetics of JG dye adsorption onto MnO_2, several models were employed, including the pseudo-first-order (PFO), pseudo-second-order (PSO), and intraparticle diffusion models. The pseudo-first-order (PFO) model, proposed by Lagergren, is represented by the following linear equation [32]:

$$Ln(q_e - q_t) = Lnq_e - K_1 t \quad (6)$$

where is the rate constant of the pseudo-first-order (PFO) adsorption, and q_e and q_t (mg/g) represent the quantities of adsorbed material at equilibrium and at time t, respectively. The values of K_1 and q_e can be determined by plotting $\ln(q_e - q_t)$ against time (t), where the slope and intercept correspond to the rate constant and equilibrium adsorption capacity, respectively. The linear form of the pseudo-second-order (PSO) model can be written as [33]:

$$\frac{t}{q_t} = \frac{1}{K_2 q_e^2} + \frac{1}{q_e} \quad (7)$$

where k_2 (g/mg. min) is the equilibrium rate constant of the PSO model. The values of k_2 and q_e can be determined from the slope and intercept of the plot of t/q_t versus time (t). The parameters for PFO and PSO models are presented in Table 1.

Table 1. The kinetic parameters of adsorption JG dye on MnO_2 NPs using PFO and PSO models at different temperatures.

T, K	PFO				PSO			
	K_1, min^{-1}	q_e (exp), $mg.g^{-1}$	q_e (cal), $mg.g^{-1}$	R^2	k_2, $g.mg^{-1}.min^{-1}$	$q_{e(exp)}$, $mg.g^{-1}$	$q_{e(cal)}$, $mg.g^{-1}$	R^2
288.15	0.0397	2.2003	1.6164	0.9387	0.0345	2.2003	2.3861	0.9977
298.15	0.0512	2.4098	1.9352	0.9156	0.0331	2.4098	2.6144	0.9945
308.15	0.0424	2.5372	1.0580	0.8905	0.0689	2.5372	2.6385	0.9989
318.15	0.0317	2.5584	0.5420	0.9311	0.1584	2.5584	2.5934	1

In comparison to the PFO kinetic model at four different temperatures, the PSO kinetic model consistently exhibited higher correlation coefficients. Additionally, the experimental $q_{e\ (exp)}$ and the calculated $q_{e\ (cal)}$ values from the PSO model showed better alignment than those obtained from the PFO model. Consequently, the adsorption kinetics of JG dye onto MnO_2 are more precisely described by the PSO model. This confirms that the adsorption of JG dye onto MnO_2 NPs is likely controlled by a chemisorption process [34]. To identify the rate-limiting step of the adsorption process, Weber and Morris proposed an intraparticle diffusion equation, which can be expressed as [35, 36]:

$$q_t = K_I t^{0.5} + C \quad (8)$$

By plotting q_t vs. $t^{0.5}$ (Figure 8) the formed slope represents the rate constant of intraparticle diffusion K_I ($mg/g.min^{0.5}$), while the formed intercept represents the thickness of the boundary layer C (mg/g). The obtained data of intraparticle diffusion parameters are summarized in Table 2.

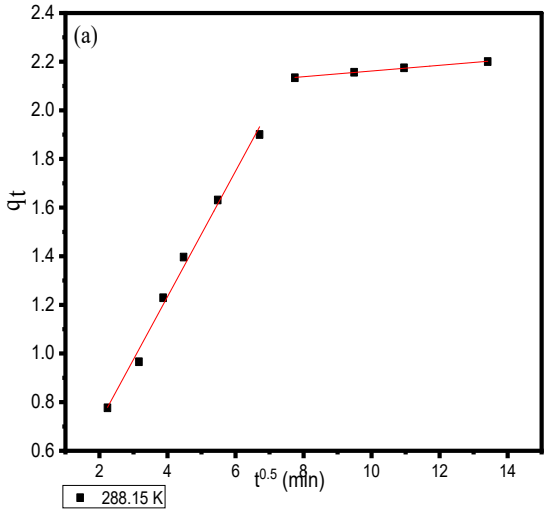

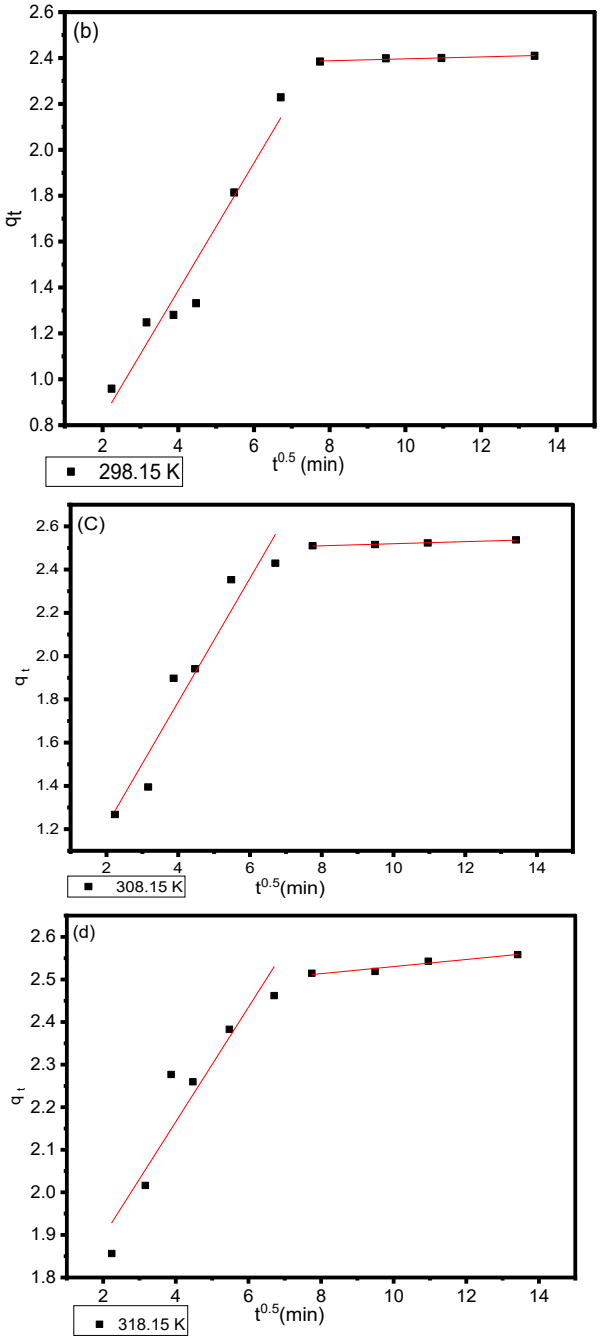

Figure 8. Intraparticle diffusion equation of adsorption JG dye on MnO_2 at different temperatures ((a) – at 288.15 K; (b) – at 298.15 K, (c) – at 308.15 K, and (d) – at 318.15 K).

Table 2. Parameters of Weber-Morris intraparticle diffusion model at different temperatures.

Kinetic parameters	Temperatures (K)			
Segment 1	288.15	298.15	308.15	318.15
C	0.20164	0.27678	0.6459	1.62789
K_1	0.25800	0.27763	0.28570	0.13447
R^2	0.99258	0.94255	0.92686	0.89036
Segment 2				
C	2.04438	2.35446	2.47166	2.44690
K_2	0.01172	0.00420	0.00480	0.00834

As depicted in Figure 8, two distinct linear regions are observed, indicating the involvement of two stages in the JG dye adsorption process. The first, more prominent region represents the external transfer diffusion, while the second linear segment corresponds to the equilibrium phase of the adsorbent ($K_2 < K_1$), indicating a decrease in the number of available adsorption sites. At this stage, intraparticle diffusion becomes the rate-limiting step [37, 38].

Calculation of activation energy and thermodynamic functions using the Eyring equation

The Arrhenius equation was applied to calculate the activation energy, which is expressed by the following equation [39]:

$$\ln k_2 = \ln A - \frac{E_a}{RT} \tag{9}$$

where k_2 (g.mg^{-1}.min^{-1}) is the pseudo-second-order reaction rate constant, R (8.314 J/mol·K) is the universal gas constant, A is the Arrhenius pre-exponential factor, and E_a (J/mol) is the activation energy. The activation energy (E_a) for MnO_2 can be determined from the slope of the linear plot of ln k_2 versus 1/T, using the equation Y = -4811.3X + 13.069, with an R^2 value of 0.8494. Based on this analysis, the calculated activation energy is 39.9 kJ/mol. This value indicates that the adsorption process is chemical in nature where the adsorbate forms stronger bonds with the adsorbent. To include additional thermodynamic factors and gain a more thorough understanding of the reaction mechanism, the linear form of the Eyring equation, derived from transition state theory (Eq. 10), was employed to calculate the thermodynamic activation parameters, including enthalpy (ΔH*), entropy (ΔS*), and free energy (ΔG*) [14]. This approach was also used to examine the effect of temperature on the transport and kinetic barriers involved in the adsorption process of JG dye.

$$ln\frac{k_2}{T} = \ln\frac{k_B}{h} + \frac{\Delta S^*}{R} - \frac{\Delta H^*}{RT} \tag{10}$$

where (K_B) is the Boltzmann constant 1.3807×10^{-23} (J/K) and (h) is the Planck constant 6.6261×10^{-34} (J s). The k_2 stands for the rate constant of PSO. Plotting ln(k_2/T) against 1/T produced a straight line. The ΔH* and ΔS* were calculated using the line's slope (-ΔH*/R) and intercept (ln k_B/h + ΔS*/R). The positive value of change in activation enthalpy (37.48 kJ/mol) indicates that this transition requires energy to occur (endothermic). A negative value of ΔS* (-144.69 J/mol) in the adsorption process of JG on a MnO_2 surface indicates that the adsorption of JG molecules onto a surface involves a more organized arrangement, such as the formation of a stable adsorbate layer. The free energy of activation (ΔG*) for the adsorption of JG was calculated using Equation 11:

$$\Delta G^* = \Delta H^* - T\Delta S^* \tag{11}$$

The calculated Gibbs free energies were 79.17, 80.62, 82.07, and 83.51 kJ/mol at temperatures of 288.15, 298.15, 308.15, and 318.15 K, respectively. The positive values of Gibbs free energy for the JG adsorption at all temperatures indicate that, in chemisorption, the activation energy is higher, as the system must overcome a greater energy barrier to form these bonds. Similar trends have been observed in other studies [14].

CONCLUSION

In this study, manganese dioxide MnO_2 was successfully prepared using the hydrothermal method. The spectral and structural characteristics of the prepared surface were studied using several techniques (XRD, FT-IR, FE-SEM, and EDX). The prepared surface was used as an adsorbent surface, and its adsorption efficiency was measured by removing JG dye from its aqueous solution, where 0.15 g of it achieved a removal rate of 87.55%. It has been demonstrated to be an efficient process, reaching adsorption equilibrium in approximately 60 min. The results obtained from studying the kinetic behavior of the adsorbent surface were more consistent with the PSO kinetic model ($R^2 > 0.99$). Through the values of the calculated thermodynamic functions, it was found that the adsorption is chemisorption, endothermic, with the formation of a stable adsorbate layer.

ACKNOWLEDGMENTS

The authors would like to express their gratitude to the College of Education for Pure Science (Ibn al-Haitham), Department of Chemistry, University of Baghdad.

REFERENCES

1. Faraj, R.A.; Abbas, A.M. Loading and activating a carbon surface and applied for congo red adsorption, kinetic study. *J. Phys. Conf. Ser.* **2021**, 1879, 1-10.
2. Rezala, H.; Romero, A.; Tidjani, N. Investigating the comparative adsorption of methyl orange and methyl green on commercial bentonite. *Bull. Chem. Soc. Ethiop*. **2025**, 39, 643-657.
3. Wasti, A.; Ali, A.M. Adsorption of textile dye onto modified immobilized activated alumina. *J. Assoc. Arab Univ. Basic Appl. Sci.* **2016**, 20, 26-31.
4. Sathya, K.; Nagarajan, K.; Carlin Geor M.G.; Rajalakshmi, S.; Raja Lakshmi, P. A comprehensive review on comparison among effluent treatment methods and modern methods of treatment of industrial wastewater effluent from different sources. *Appl. Water Sci.* **2022**, 12, 1-27.
5. Katheresan, V.; Kansedo, J.; Lau, S. Y. Efficiency of various recent wastewater dye removal methods: A review. *J. Environ. Chem. Eng.* **2018**, 6, 4676-4697.
6. Bożęcka, A.; Orlof-Naturalna, M.; Kopeć, M. Methods of dyes removal from aqueous environment. *J. Ecol. Eng.* **2021**, 22, 111-118.
7. Sabbar, H.A.; Noori, W.O.; Naje, A.S. Dye removal by membrane technology for wastewater treatment using a cationic carrier. *Pertanika J. Sci. Technol*. **2020**, 28, 353-397.
8. Cordier, C.; Charpin, L.; Stavrakakis, C.; Papin, M.; Guyomard, K.; Sauvade, P.; Coelho, F.; Moulin, P. Ultrafiltration: A solution to recycle the breeding waters in shellfish production. *Aquac. Res.* **2019**, 504, 30-38.
9. Ahmed, A.E.; Majewska-Nowak, K.; Ahmed, M.; Grzegorzek, M. The separation of mineral salt from a dye-salt aqueous mixture by electrodialysis. *Desalin. Water Treat*. **2023**, 316, 532-541.
10. Sadoon, Z.A.; M-Ridha, M.J. Removal of reactive dyes by electrocoagulation process from aqueous solution. *J. Eng.* **2020**, 26, 14-28.

11. Al-Jadabi, N.; Laaouan, M.; Benbouzid, M.; Mabrouki, J.; El Hajjaji, S. Coagulation-flocculation technique for domestic wastewater treatment in the city of Ain Aouda, Rabat, Morocco. *E3S Web Conf.* **2022**, 337, 1-9.
12. Al-Hazmi, G.H.; Adam, A.A.; El-Desouky, M.G.; El Bindary, A.A.; Alsuhaibani, A.M.; Refat, M.S. Efficient adsorption of rhodamine B using a composite of Fe_3O_4@ZIF-8: synthesis, characterization, modeling analysis, statistical physics and mechanism of interaction. *Bull. Chem. Soc. Ethiop*. **2023**, 37, 211-229.
13. Alkan, M.; Celikcapa, S.; Demirbas, Ö.; Dogan, M. Removal of reactive blue 221 and acid blue 62 anionic dyes from aqueous solutions by sepiolite. *Dyes Pigm.* **2005**, 65, 251-259.
14. Abduljabar, M.A.; Merza, S.H. Synthesis, characterization of nickel cobaltite nanoparticles and its use in removal methyl green dye from aqueous solution. *IHJPAS* **2024**, 37, 264-278.
15. Khuntia, S.; Majumder, S.K.; Ghosh P. Catalytic ozonation of dye in a microbubble system: hydroxyl radical contribution and effect of salt. *J. Environ. Chem. Eng*. **2016**, 4, 2250-2258.
16. Nawaz, F.; Xie, Y.; Xiao, J.; Cao, H.; Ghazi, Z.A.; Guo, Z.; Chen, Y. The influence of the substituent on the phenol oxidation rate and reactive species in cubic MnO_2 catalytic ozonation. *Catal. Sci. Technol.* **2016**, 6, 7875-7884.
17. Tan, X.; Wan, Y.; Huang, Y.; He, C.; Zhang, Z.; He, Z.; Hu, L.; Zeng, J.; Shu, D. Three-dimensional MnO_2 porous hollow microspheres for enhanced activity as ozonation catalysts in degradation of bisphenol A. *J. Hazard. Mater.* **2017**, 321, 162-172.
18. Abdel S.M. Synthesis and characterization of novel manganese oxide nanocorals and their application for the removal of methylene blue from aqueous solution. *Chem. Eng. J.* **2015**, 270, 50-57.
19. Saeed, T.; Naeem, A.; Mahmood, T.; Ahmad, Z.; Farooq, M.; Farida, Din, I.U.; Khan, I.W. Comparative study for removal of cationic dye from aqueous solutions by manganese oxide and manganese oxide composite. *IJEST* **2021**, 18, 659-672.
20. Nagda, G.K.; Ghole, V.S. Removal of Janus green dye from aqueous solution by phosphoric acid carbonized agro-industrial waste. *Sci. Asia*. **2011**, 37, 38-42.
21. Merza, S.H.; Abdul, I. Synthesis of modified graphene oxide and its application as electrochemical sensor. PhD Thesis, University of Baghdad, Iraq, Baghdad, **2016**.
22. Kang, L.; Zhang, M.; Liu, Z. H.; Ooi, K. IR spectra of manganese oxides with either layered or tunnel structures. *Spectrochim. Acta A Mol. Biomol. Spectrosc*. **2007**, 67, 864-869.
23. Yugambica, S.; Dhanemozhi, C. A.; Iswariya, S. Synthesis and characterization of MnO_2/rGO nanocomposite for supercapacitors. *IRJET* **2017**, 4, 486-491.
24. Coates, J.P. The interpretation of infrared spectra: published reference sources. *Appl. Spectrosc. Rev*. **1996**, 31, 179-192.
25. Davoglio, R.A.; Cabello, G.; Marco, J.F.; Biaggio, S.R. Synthesis and characterization of α-MnO_2 nanoneedles for electrochemical supercapacitors. *Electrochim. Acta.* **2018,** 261, 428-435.
26. Merza, S.H.; Mousa, E.F. Dielectric properties of ultra-low dielectric constant PVA-pentaerythritol/MnO_2 nanocomposite. *Phys. Chem. Res.* **2022**, 10, 325-331.
27. Kadhim, H. H.; Saleh, K. A. Removing cobalt ions from industrial wastewater using chitosan. *Iraqi J. Sci.* **2022**, 63, 3251-3263.
28. Sultan, M.S.; Radi, M.F.; Jasim, A.A.; Tahir, J.S.; Abdul Ghani, L.H.; Maryoosh, A.A.; Abdul abass, D.A. Removing of hexavalent chromium from aqueous solutions using dried yogurt, and studying isotherm, kinetic and thermodynamic parameters. *Baghdad Sci. J*. **2019**, 16, 603-609.
29. Farhan, A.M.; Zaghair, A.M.; Abdullah, H.I. Adsorption study of rhodamine B dye on plant (citrus leaves). *Baghdad Sci. J*. **2022**, 19, 838-847.
30. Al-Shammari, N.H.; Al-Mammar, D.E. Adsorption of biebrich scarlet dye into remains chromium and vegetable tanned leather as adsorbents. *Iraqi J. Sci.* **2022**, 63, 2814-2826.

31. Dong, W.F.; Zang, L.; Li, H. Application of MnO_2 materials to dye removal from aqueous solution by adsorption *AMM.* **2013,** 361-363, 760-763.
32. Ibrahim, N.H.; Al-Jubouri, S.M. Green porous composite for combining ion exchange-adsorptive removal of zinc ions from aqueous solutions. *Iraqi J. Sci.* **2024**, 65, 6229-6241.
33. Jawad, A.H.; Saber, S.E.M.; Abdulhameed, A.S.; Farhan, A.M.; Al Othman, Z.A.; Wilson, L.D. Characterization and applicability of the natural Iraqi bentonite clay for toxic cationic dye removal: Adsorption kinetic and isotherm study. *J. King Saud Univ. Sci.* **2023**, 35, 102630.
34. Liu, M.; Yin, W.; Zhao, T.L.; Yao, Q.Z.; Fu, S.Q.; Zhou, G.T. High-efficient removal of organic dyes from model wastewater using $Mg(OH)_2$-MnO_2 nanocomposite: synergistic effects of adsorption, precipitation, and photodegradation. *Sep. Purif. Technol.* **2021**, 272, 1-9.
35. Abbas, A.M.; Merza, S.H. Preparation and characterization of graphene oxide – attapulgite composite and its use in kinetic study of alizarin dye adsorption from aqueous media. *Egypt. J. Chem*. **2020**, 63, 561-572.
36. Konicki, W.; Hełminiak, A.; Arabczyk, W.; Mijowska, E. Removal of anionic dyes using magnetic Fe@graphite core-shell nanocomposite as an adsorbent from aqueous solutions. *J. Colloid. Interface Sci*. **2017**, 497, 155-164.
37. Abduljabar, M.A.; Merza, S. H. Graphene oxide decorated with nickel cobaltite nanoparticles as an adsorbent for cationic methyl green dye: kinetic, isotherm, and thermodynamic studies. *Baghdad Sci. J*. **2024**, 21, 2853-2865.
38. Pholosi, A.; Naidoo, E.B.; Ofomaja, A. E. Intraparticle diffusion of Cr (VI) through biomass and magnetite coated biomass: a comparative kinetic and diffusion study *S. Afr. J. Chem. Eng.* **2020**, 32, 39-55.
39. Muhi-Alden, Y.Y.; Saleh, K.A. Removing of methylene blue dye from its Aqueous Solutions using polyacrylonitrile/iron oxide/graphene oxide. *Iraqi J. Sci*. **2022**, 63, 2320-2330.